Heteroaggregation and Selective Deposition for the Fine Design of Nanoarchitectured Bifunctional Catalysts: Application to Hydroisomerization

Olfa Ben Moussa, Lionel Tinat, Xiaojing Jin, Walid Baaziz, Olivier Durupthy, Celine Sayag, Juliette Blanchard

Heteroaggregation and selective deposition for the fine design of nanoarchitectured bifunctional catalysts: application to hydroisomerization.

Olfa Ben Moussa,[†, ‡] Lionel Tinat,[†, ‡] Xiaojing Jin[†], Walid Baaziz[§], Olivier Durupthy,[*, ‡] Céline Sayag[†] and Juliette Blanchard*,[†]

† Sorbonne Université, CNRS, Laboratoire de Réactivité de Surface, LRS UMR 7197, F-75005, Paris, France.

‡ Sorbonne Université, CNRS, Collège de France, Laboratoire de Chimie de la Matière Condensée de Paris, LCMCP, F-75005, Paris, France

§ Institut de Physique et Chimie des Matériaux de Strasbourg (IPCMS), UMR 7504 CNRS, Université de Strasbourg, 23 rue du Loess, F-67037 Strasbourg, France

ABSTRACT: We successfully prepared bifunctional catalysts with the distance between metallic and acid sites tuned at the nanometer scale. Sols of beta zeolite nanoparticles were synthesized and mixed in optimized conditions with a γ-AlOOH boehmite suspension in order to yield alumina/zeolite aggregates with a nanometer scale intimacy. The composition of the aggregate could be tuned from pure alumina to pure zeolite. Then, by careful choosing the Pt precursor and the pH conditions, we were able to selectively deposit platinum, either on alumina or in zeolite domains. A subsequent, soft thermoreduction step was applied that produced well-dispersed Pt nanoparticles either on alumina or in the zeolite nano-domains as confirmed by 3D tomography microscopy experiments. The catalytic properties of the obtained nanostructured catalysts were studied through n-heptane conversion. Comparison of these original bifunctional catalysts with monofunctional or conventional bifunctional catalysts showed the impact of the location of the metallic particles on the selectivity.

KEYWORDS: heterocoagulation, nanozeolites, boehmite, platinum nanoparticles, bifunctional catalyst, hydrocracking/hydroisomerization

I. INTRODUCTION

Zeolites are widely used in bifunctional acid-metal catalysis, where they play the dual role of support for the metallic particles and source of Brønsted acid sites [1]. However, the microporosity of zeolites results in internal diffusion limitations which can impact negatively the activity. To alleviate these diffusion limitations, the diffusional path length in the micropores should be kept very short, for example by creating a secondary network of larger pores (in the mesopore range) [2] or by using nanometer-size zeolite particles [3]. A promising alternative has been recently proposed by Zecevic et al.: they took advantage of the fact that commercial zeolite extrudate contains, beside the zeolite, a binder, usually alumina, that can be used as an alternative support for the metallic particles [4]. These authors demonstrated that a location of the platinum nanoparticles on the binder has, despite the higher distance between metallic and acid sites, a positive effect on the selectivity toward isomerisation, without repercussion on the activity.

In the present work, we intended to explore another scale of intimacy between metallic and acid sites by preparing nanometer-scale and micrometer scale beta zeolite-alumina support, on which platinum nanoparticles (**Pt° NPs**) are selectively formed either on the alumina domains or in the zeolite particles. This fine design allows a better accessibility of both metallic and acidic sites and a better control on their vicinity and hence a better understanding of the role of these two parameters on the activity and selectivity of bifunctional catalysts for the model reaction of n-heptane hydrocracking.

II. EXPERIMENTAL SECTION

II.1. Preparation of the catalysts

Synthesis of beta zeolite nanoparticles. The protocol we followed was adapted from the literature. [5-6] 4.90 g (0.024 mol) of aluminum isopropoxide (AIP) were first dissolved in 246 mL of water and 95.7 g of 35 % aqueous tetraethylammonium hydroxide (TEAOH). 131.5 g of TEOS were added (pH = 11.8) and the mixture was stirred for 72 h (the solution became clear after ca. 3 h). The molar composition at this step is *18 TEAOH : Al_2O_3 : 50 SiO_2 : 1000 H_2O.* An evaporation step was performed to remove ethanol and excess water in a rotary evaporator (Büchi) operated first at 50 °C and 100 mbar for 3 h then at 80 °C and 70 mbar for 7 min. When the targeted R = H2O/SiO2 ratio of 7 was reached, the solution, which was still transparent, turned viscous. The sol was transferred in a closed glass vial for hydrothermal treatment in an oven at 90 °C for 133 h. To decrease its viscosity, the suspension was diluted (1 mL of

suspension in 8 mL of water) and the solid phase was collected by centrifugation (27000 rpm, 30 min) and redispersed twice in distilled water (with, after each redispersion, a centrifugation at 27000 rpm during 30 min to recover the colloidal particles). The zeolite particles were either dried in an oven at 60 °C overnight or redispersed in water for future use.

Preparation of Zeolite-alumina aggregates by heterocoagulation. Boehmite PURAL SB3 (SASOL) nanoparticles were dispersed in 45 mL of HCl solution (0.12 mol L^{-1}). A good dispersion was obtained after 2 h of magnetic stirring (1000 rpm) followed by 30 min of ultrasonication. The suspension was then diluted to a concentration of 10 g L^{-1} and the pH was set to 6.0 by adding small doses of a sodium hydroxide solution (1.0 mol L^{-1}). The above prepared zeolite suspension was also diluted in a 1 – 25 g L^{-1} concentration range and its pH was set to 9.0 using an HCl aqueous solution (0.1 mol L^{-1}). Equal volumes of the boehmite and zeolite suspensions were mixed through dropwise addition of the less concentrated suspension into the more concentrated one under vigorous stirring (800 rpm). The suspension was then left without stirring for one hour and the solid phase was collected through centrifugation. This centrifugation was performed at moderate speed (9000 rpm, 15 min) in order to ensure that only the heteroaggregates were collected during this step, while unaggregated zeolite and boehmite nanoparticles remained in the solution. The powder was dried in an oven overnight at 60 °C and then calcined at 550 °C in a muffle furnace for 4 h (1.5 °C min^{-1} heating rate). During this step the boehmite is converted to alumina and the template is removed from the zeolite. These composites are named **nm-composites**.

Preparation of Zeolite-alumina aggregates by wet mechanical mixing (kneading). 0.7 g of boehmite (PURAL SB3) and 0.3 g of commercial zeolite (NH4-BEA, Si/Al=20.5, Alfa Aesar, average particle size ca. 0.5 µm, see Figure S1) were mechanically mixed with 1 mL of distillated water for 1 min. The paste was dried and calcined according to the same procedure as that described above. This composite is named **µm-composite**.

Preparation of Pt°/Al_2O_3-zeolite. The alumina-zeolite composite (either nm- or µm- composite) was dispersed in water (1.00 g in 400 mL) for 1 h under vigorous stirring. In parallel, 0.238 g of a 8.8 wt% H_2PtCl_6 aqueous solution(corresponding to 10 mg of platinum) was diluted in 50 mL of distilled water (pH≈4). The Pt precursor solution was added dropwise to the suspension under stirring and the stirring was maintained for 3 h. The solid phase was collected through centrifugation, washed with distilled water and dried under vacuum for 24 h at 35 °C. The powder was calcined under O_2 flow (1 L min^{-1} g^{-1}) at 150 °C for 2 h with a heating ramp of 1 °C min^{-1}. For the formation of the platinum nanoparticles, 0.1 g of Pt/γ-Al_2O_3-zeolite was heated under H_2 flow (25 mL min^{-1}, 2 °C min^{-1} heating ramp with an intermediate plateau at 150 °C during 20 min and a final plateau at 400 °C during 2 h). Samples prepared with an initial location of platinum on the alumina domains are named **Pt/A-(µm or nm)**-composite.

Preparation of Pt°/zeolite-Al_2O_3. The alumina-zeolite aggregate was dispersed in water (1.00 g in 400 mL) for 1 h under vigorous stirring. In parallel, 0.020 g of $Pt(NH_3)_4(NO_3)_2$ (equivalent to 10 mg of platinum) was solubilized in 50 mL of distilled water. The Pt precursor solution was added dropwise to the suspension under stirring and the stirring was maintained for 3 h (final pH=5). The solid phase was collected through centrifugation, washed with distilled water and dried under vacuum for 24 h at 35 °C. The sample was calcined under O_2 flow (1 L min^{-1} g^{-1}) at 350 °C for 2h with a heating ramp of 0.2 °C min^{-1} g^{-1} and an intermediate plateau of 10 min at 100 °C. This calcination protocol is derived from the study of de Graaf et al. [7] and ensure a high dispersion of the metallic phase after the reduction step. The reduction treatment is the same as that described above. Samples prepared with an initial location of platinum on the zeolite domains are named **Pt/Z-(µm or nm)**-composite

II.2 Characterization

Crystalline structures were explored using X-Ray diffraction (XRD) performed on a Bruker D8 ADVANCE diffractometer using filtered Cu K_α radiation over a 2θ range from 6° to 42° with a step size of 0.02° and a step time of 2 s per step. Dynamic light scattering (DLS) and ζ-potential measurements were done on diluted solutions (~ 1 g L^{-1}) using a Malvern Zetasizer nanoZS90 apparatus. Particles, heteroaggregates and Pt-loaded heteroaggregates were observed in transmission electron microscopy on dried or calcined powders using a FEI Tecnai Spirit G2 instrument at an acceleration voltage of 120.0 kV, or a JEOL 1011 operating at 100 kV or a JEOL JEM 2100F operating at 200 kV. Boehmite-zeolite aggregates were also observed using cryo-TEM on the Technai Spirit G2.

The HAADF-STEM (high-angular annular dark field in scanning transmission electron microscopy) analyses were carried out using a JEOL 2100 FEG (field emission gun) S/TEM microscope operated at 200 kV equipped with a spherical aberration corrector on the probe-forming lens.

For Electron Tomography (ET), the tilt series was acquired by the tomography plug-in of the Digital Micrograph software, by using the ADF and BF detectors. The specimen was tilted in the angular range of ± 70° using an increment of 2° in the equal mode. The recorded images of the tilt series were spatially aligned by cross correlating consecutive images using IMOD software. For the volume calculation, we have used the algebraic reconstruction technique (ART) implemented in the TomoJ plugin working in the ImageJ software were thus used to compute the reconstructed volumes. The elemental composition of the catalysts was determined by X-ray fluorescence spectroscopy (XRF) using a XEPOS spectrometer (AMETEK). N_2 adsorption-desorption isotherms were collected on a Belsorp Max

(Bel Japan). Prior to analysis, the samples were degassed under primary vacuum at 300 °C for at least 6 h. The total surface area was estimated using the BET model.

Zeolite surface acidity was evaluated by FTIR of adsorbed pyridine. FTIR spectra were obtained on a Bruker Vector 22 FT-IR spectrometer (resolution: 4 cm^{-1}). ca. 15 mg of sample was pressed into a 2 cm^2 self-supported wafer), heated at 450 °C for 2 h in O_2 (P_{O_2}= 13.3 kPa) and evacuated afterward for 1h at this temperature. Pyridine (P = 133 Pa) was introduced at RT and desorbed under vacuum at 150 °C. A spectrum was recorded before adsorption of pyridine and another one after desorption at 150 °C. Pyridine adsorbed on both Lewis and Brønsted acid sites was detected. The number of acid sites (Brønsted or Lewis) was calculated based on the area of the band at 1454 cm^{-1} (Lewis) and 1546 cm^{-1} (Brønsted) and using the molar absorption coefficients determined by Guisnet et al. (1.28 cm μmol^{-1} for the band at 1454 cm^{-1} and 1.13 cm μmol^{-1} for the band at 1546 cm^{-1}). [8]

Pt dispersion was determined through the measurement of H_2 chimisorption isotherms on a Belsorp-max set-up (Bel Japan). ca. 0.1 g of catalyst was reduced *in situ* using the reduction protocol described above. After an evacuation at 400 °C under vacuum during 2 h, the reactor was placed in a thermostated bath at 25 °C and a first H_2 sorption isotherm was measured. After an evacuation step of 1 h under secondary vacuum, a second H_2 sorption isotherm was measured. The H_2 chemisorption isotherm was obtained by the difference of these two isotherms and the dispersion was determined using the Langmuir model.

II.3 Catalytic test

Catalytic conversion of n-heptane (n-C_7) was performed at 220 °C and at atmospheric pressure in a U-shaped flow-type, fixed-bed, glass tube reactor. A mass of 0.1 to 0.4 g of catalyst powder was supported on quartz wool. Prior to reaction, the catalyst was reduced *in situ* using the reduction protocol described above. The reactants (n-C_7 and H_2) were introduced by flowing H_2 through a saturator containing n-C_7 and maintained at 12.5 °C using a thermostated bath (H_2/n-C_7 mole ratio of 33:1). Mass flow rates were regulated using Brooks controllers. Effluents were analyzed by online gas chromatography (capillary column CP-Sil PONA CB, 50 × 0.21 mm, Varian) using a flame ionization detector (FID). After 22 h time-on-stream, the space velocity was adjusted by changing H_2 flow rate in order to reach conversions of 20.5% ± 2% and 50% ± 4%. Product selectivity was calculated at this conversion.

The reaction products were divided into three categories: (a) monobranched n-heptane isomers (3-ethylpentane as main product with small quantities of 2- & 3-methylhexane), denoted as **isom-mono**; (b) dibranched n-heptane isomers (2,2-, 2,4- 2,3- dimethylpentane as main products with small quantities of 3,3-dimethylpentane), denoted as **isom-di**; (c) cracking products, denoted as **cracking** (for the cracking products, only the main fragment was considered in this calculation). Equations used to calculate conversions and selectivities are as follows:

$$conversion = \frac{\sum S_{produits}}{S_{n-hep\tan e} + \sum S_{produits}} \quad selectivity(product_i) = \frac{S_{product(i)}}{\sum S_{products}}$$

For purpose of comparison, conversions were calculated for 10 µmol of Brønsted acid sites.

III. RESULTS AND DISCUSSION

III.1. Preparation of the colloidal suspension of beta zeolite nanoparticles. As previously observed by Fang et al [5], the high concentration of the synthesis gel favours nucleation over growth and hence produces, with a high yield, (ca. 50%) beta zeolite nanoparticles with good crystallinity and no impurity (ICDD file 00-047-0183) as shown by X-Ray diffraction (Figure 1-a) and TEM (Figure 2-a). Broad diffraction lines are observed on the diffractogram corresponding to a crystalline domain of ca. 10 nm based on Scherrer formula applied on (302) line(2θ=22.1°). TEM micrograph of the beta zeolite NPs (dried-uncalcined sample), shows the presence of ca. 20 nm large particles of ill-defined shape on which lattice fringes are visible indicating their good crystallinity. Based on the TEM image, it is difficult to judge of their aggregation but the hydrodynamic diameter of 33 nm (based on DLS measurements), is consistent with a very weak degree of agglomeration.

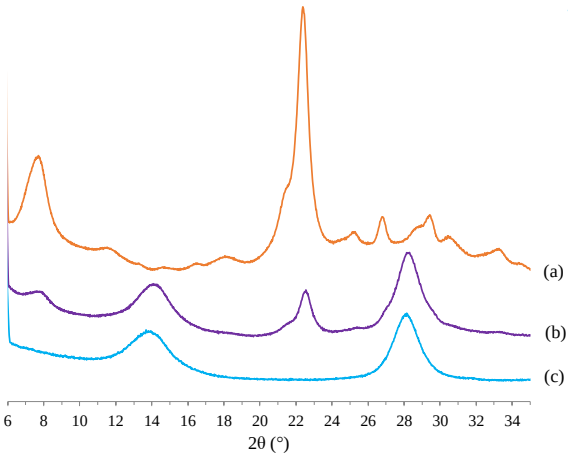

Figure 1: X-Ray diffraction patterns of a) synthesized beta zeolite nanoparticles (ICDD : 00-047-0183), b) γ-AlOOH-beta zeolite 70wt%-30wt.% heteroaggregates, and c) commercial γ-AlOOH boehmite nanoparticles (ICDD : 01-083-1505)

The Si/Al ratio measured by X-ray fluorescence spectroscopy is 17, a value lower than the composition of the reaction medium (Si/Al=25). This difference in the composition of the synthesis gel and in the final material is consistent with previous reports [5, 9-10]. For specific surface area and acidity measurements, a calcination procedure similar to that of the composite was applied to small aliquots of dried zeolite withdrawn from the suspension. The surface

area of the zeolite nanoparticles is 750 $m^2 g^{-1}$, which is significantly higher than the 608 $m^2 g^{-1}$ of the commercial beta zeolite used for the composite prepared by wet mechanical mixing. The comparison of the adsorption isotherms of the zeolite nanoparticles and of the commercial zeolite (Figure S2) indicates that this higher surface area is related to the presence of mesoporous and external surface area, in agreement with the small size of the zeolite particles in the synthesized sample. The density of Brønsted acid sites (FTIR of adsorbed pyridine) is 124 μmol g^{-1}. This value is significantly lower than the Al content (930 μmol g^{-1}), indicating that not all Al atoms contribute to the Brønsted acidity. In agreement with this, the presence of Lewis acid sites (138 μmol g^{-1}) was also detected by this method. A similarly lower-than-expected density of Brønsted acid sites in nm-size beta zeolite particles has been previously reported by Astafan et al. [3].

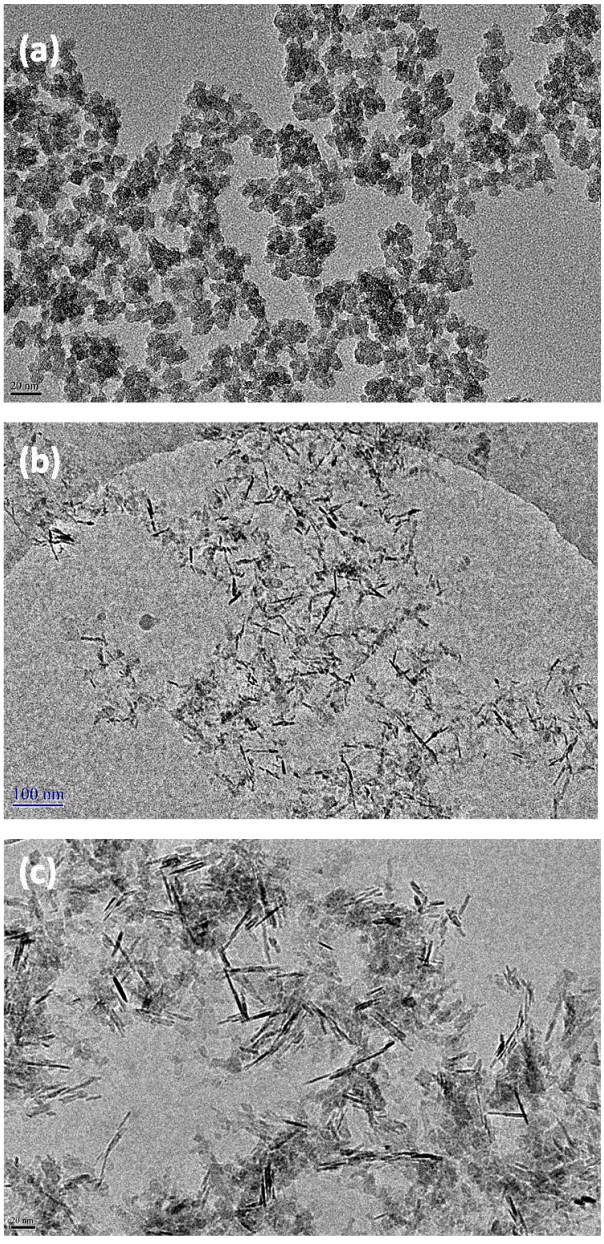

Figure 2: a) TEM image of synthesized beta zeolite nanoparticles (scale bar 20 nm); b) Cryo-TEM image of the colloidal suspension of commercial SB3 γ-AlOOH (boehmite) nanoparticles (scale bar 100 nm); (c) Cryo-TEM image of the colloidal suspension of SB3-beta 75%-25% (scale bar 20 nm);

III.2. Formation of zeolite-boehmite composites by heterocoagulation. Our target is to prepare alumina-zeolite composite at the nanometer scale for the selective deposition of platinum either on the alumina or in the zeolite nanoparticles. In order to reach a nanometer scale intimacy between these two components, we have chosen to use, as alumina precursor, γ-AlOOH nanoparticles. Dispersion state of commercial Pural SB3 particles was estimated through cryo-TEM observation of the suspension (see Figure 2b). Aggregates of less than 50 nm are observed, consisting of bundles of platelets (that appear either as platelet or as needles on the TEM image depending on their orientation) less than 5 nm thick. The hydrodynamic diameter of the aggregates is 40 nm based on DLS while crystallite thickness measured using Scherrer equation on (020) diffraction line at $2\theta = 14.5°$ (XRD pattern reported in Figure 1c) is 4 nm. The evolution of the ζ-potential of the boehmite suspension as a function of the pH is reported in Figure S3. An isoelectric point at pH = 9.1 is observed which is fair agreement with previous results. [11] Below this pH value, the boehmite nanoparticles are positively charged and the ζ-potential is higher than 25 mV in the 3-8 pH range confirming colloidal stability. The same ζ-potential study on beta zeolite nanoparticles, also reported in Figure S3, gave negative values in the whole 3-11 pH range. The fact that the beta zeolite surface is negatively charged over a wide range of pH is expected as templated beta zeolite may be assimilated to a pure silica surface which is indeed negatively charged up to pH = 2. The surface ζ-potential is below -25 mV for suspension at pH ≥ 6.

The choice of the mixing pH range from 6 to 9 is then motivated by the presence of significant amount of opposed surface charges on boehmite and zeolite nanoparticles. Moreover, the order of mixing is part of the strategy in the design of isolated nano-heterostructure. Indeed, when introducing the minor component of the composite into a suspension of the major component, it is immediately coated with the secondary phase and presents the same surface charge sign as the major component. Depending on the relative amount of the two components used for heteroaggregation, we have obtained boehmite platelets sandwiched by zeolite nanoparticles (Figure S4-a) or zeolite nanoparticles decorated with boehmite platelets (Figure 2-c and S4-b&c). In the latter case, the obtained heteroaggregates where boehmite needles are surrounding the zeolite nanoparticles. Some boehmite nanoparticles bundles (less than 10 crystallites) can be observed in close contact with rounder shape zeolite particles or small aggregates. The maximum distance observed on the cryo-TEM image between a boehmite domain and a zeolite one is less than 50

nm. Consequently, the electrostatic interaction of oppositely charged surfaces yields intimately mixed heteroaggregates. In addition, the γ-AlOOH rich composites form stable suspensions with a ζ-potential above 25 mV for composition higher than 50 wt.% in boehmite, whereas the beta zeolite rich suspension tend to form large aggregates with a weakly negative ζ-potential (ca. 10 mV). The XRD patterns of the composites (Figure 1-b and Figure S5) confirm the presence of both crystalline components. A quantification based on the mechanical mixing of beta zeolite and boehmite powders allowed to determine the effective composition of the heteroaggregates. For instance, a 75 wt.% load of boehmite is found in the composite with a targeted composition of 70 wt.%.

III.3. Preparation of bifunctional catalysts. The heteroaggregation in aqueous solution of beta zeolite and γ-AlOOH boehmite nanoparticles allowed mixing the two components at the ten nanometer scale. Another composite was prepared in this study through wet mechanical mixing of commercial beta zeolite and boehmite powders in a minimum of water. The composites were then calcined prior to metallic phase deposition in order to clear the zeolite porosity of its template and transform γ-AlOOH into γ-Al_2O_3. The XRD patterns of the calcined composites confirm that the crystallinity of the zeolite nanoparticles is preserved after calcination (Figure S5). The shape of N2-sorption isotherm of the Al_2O_3-Beta 70-30 nm-composite (Figure S6) is consistent with the presence of the zeolite and the alumina component. The calcined composites were also analysed in terms of specific surface and surface acidity and the corresponding values (reported in Table 1) were compared to that of pure beta zeolite (nanometric and commercial) and boehmite nanoparticles calcined separately.

Table 1: compositions, surface areas and Bronsted acidities of the nm-scale and µm scale composites and of their components

	nm-Beta	nm-composite		µm-Beta	µm-composite	Al_2O_3
% $AlOOH_{synth}$	-	50	70	0	75	-
% $AlOO_{XRD}$	-	65	75	0	75	-
% Al_2O_3	0	61	72	0	72	100
S_{BET} ($m^2.g^{-1}$)	750	433	322	608	399	200
S_{micro} ($m^2.g^{-1}$)	466	175	109	466	185	35
Bronsted Acidity (µmol g^{-1})	124	-	56	288	101	-

As one could expect, the BET surface areas and acidities of the composites are similar (within 20%) to the weighted average of the BET surface areas or acidities of their two components. The zeolite/Al_2O_3 mixing level was also determined using TEM and the micrographs, reported in Figure S7, clearly show that the tens nm scale intimacy of the composite formed through heteroaggregation is preserved after the calcination step. Oppositely, the composite prepared by wet mechanical mixing displays hundreds of nanometers domains where zeolite and alumina are segregated from one another.

The two composites were used for the selective formation of Pt nanoparticles either on the zeolite or alumina component, by selecting the appropriate platinum precursor. The experimental conditions are adapted from the literature [12] and are optimized to yield highly regioselective formation of Pt nanoparticles with a good dispersion state on the targeted support. For instance we used, for the formation of platinum nanoparticles selectively on the alumina support, a negatively charged platinum precursor and conducted its adsorption at low pH (pH = 3-4). Indeed, in this pH range, an electrostatic interaction (so called SEA, strong electrostatic adsorption [13]) occurs between the positively charged alumina surface (as the Point of Zero Charge (PZC) of alumina is ca. 9) and the negatively charged $[PtCl_6]^{2-}$ complex. Moreover, the adsorption of this negatively charged complex in the zeolite is negligible as the silanols are also negatively charged at this pH. Conversely, for the formation of the platinum particles selectively in the zeolite domains, we used a positively charged platinum complex and performed its adsorption at-pH≈5~~-a neutral pH~~. Under these conditions, an ion exchange reaction occurs between the protons (Brønsted acid sites) of the zeolite and the platinum precursor. Moreover, in this pH range the alumina surface is positively charged and hence, the adsorption of the cationic complex on it is negligible. Furthermore, the adsorption of the platinum precursor on silanols groups at the external surface of the zeolite particles can also be regarded as negligible[12]. Another important point, especially for the samples prepared by ion exchange of $Pt(NH_3)_4^{2+}$ in the zeolite, is the calcination step prior to metal reduction that must be adapted to the Pt precursor. As previously reported by de Graaf et al, inappropriate calcination conditions will result in a poor dispersion, due to a too high mobility of the platinum species during this step [7]. Keeping the mobility of the platinum species as low as possible at all steps of the preparation of the catalyst is of paramount importance in our study, not only for obtaining a catalyst with a high platinum dispersion, but also because this mobility could result in the undesired migration of platinum particles on the second component. Dispersion of the metallic phase on the catalysts was investigated by means of H_2 chemisorption. The values are reported in Table 2. A high dispersion was observed for all catalysts. This high dispersion corresponds to small particle size and hence to a small number of platinum atom per particle (about 80 atoms per particle for a dispersion of ca. 75% and about 180 atoms for a dispersion of ca. 55% [7]). This small number of platinum atoms per metallic particle is already a good indication of moderate platinum diffusion during the calcination and reduction steps

and hence point out toward the formation of the platinum particles on the same component where the platinum precursor had been deposited.

Table 2: platinum loading (XRF) and platinum nanoparticles sizes and dispersions (H_2-chemisorption) for the tested catalysts.

	Pt (wt%)	$\emptyset H_2$ (nm)	DH_2 (%)	C_{Pt} ($\mu mol\ g^{-1}$)
Pt/Al_2O_3	0.75	2.1	52.5	20.2
Pt/A-µm-comp.	0.77	2.1	54.7	21.6
Pt/A-nm-comp.	1.04	1.5	76	40.5
Pt/Z-µm-comp.	0.9	2.0	56	25.8
Pt/Z-nm-comp.	0.4	1.5	76	15.6

Pt/A stands for catalysts with a location of the platinum NPs on the alumina domains and Pt/Z for their location in the zeolites particles.

In order to investigate the position of platinum nanoparticles within the support, Electron Tomography (ET) experiments were carried out on the two catalysts prepared by depositing the platinum precursor either on the alumina or on the zeolite domains of the nanocomposite. Unlike conventional 2D TEM images, ET allows a 3D visualization of the objects, which is of important interest in our case: indeed, when the signal from alumina and zeolite nanoparticles are stacked on the same plan (as the case of 2D projections images), it is impossible to conclude regarding the location of a Pt nanoparticle on the supports. This could be resolved by ET tomography which gives the possibility to analyse the composites through slices extracted from the calculated 3D volumes and provides thus a precise location of Pt nanoparticles on the alumina/zeolite support. Tilted images for ET were recorded in STEM (Scanning-TEM) imaging mode to obtain a contrast depending from the chemical nature of elements. Figure 3 presents STEM images and typical slices extracted from the calculated volumes obtained for two representative Pt/A-nm and Pt/Z-nm composites (more results are present in Figure S8).

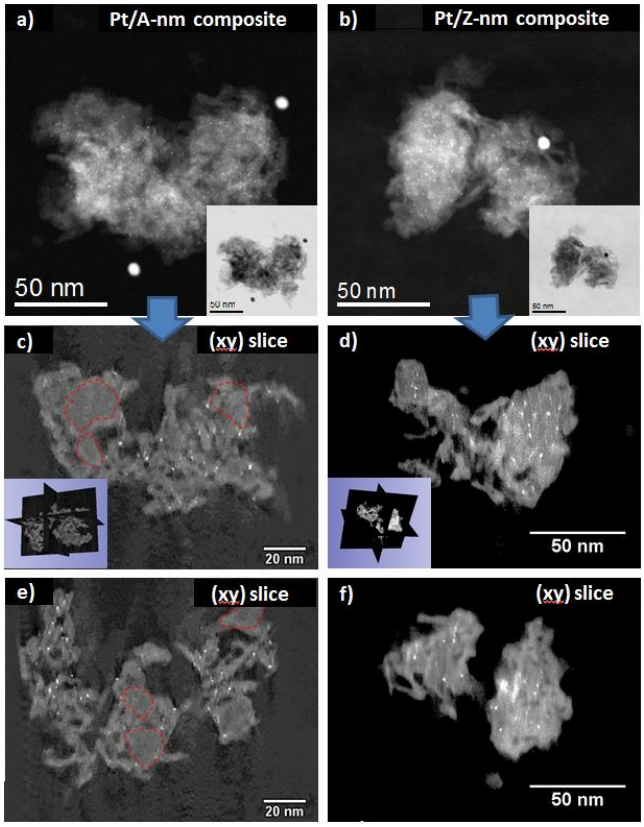

Figure 3: STEM images of the two nm-composites Pt/A-nm comp. a), c), e) and Pt/Z-nm comp b), d), f). a) and b) are dark field images (with the corresponding bright field images in inset) c-e) are slices extracted from the reconstructed 3D volume (some orthogonal slices from the obtained 3D volume are present in inset in c) and d). Highly contrasted spherical objects observed in first two micrographs are gold nanoparticles added for the alignment purpose of the tilt series.

The images for ET were recorded in bright field (BF) and dark field (DF) simultaneously, the 3D volume was calculated from the DF images, which allow a better observation of small Pt nanoparticles. In such imaging mode it is difficult to distinguish between alumina and zeolite particles which have almost the same contrast, but they could be identified thruogh ttypical shape, i.e rod-like shape alumina nanoparticles and fluffy domains of zeolite nanoparticles. For the Pt/A-nm composite, the typical slices shown in Figure 3 show clearly that Pt nanoparticles are located only on alumina domains and that zeolite domains are Pt free (highlighted by red lines). Oppositely, in the Pt/Z-nm comp. sample, the Pt particles are observed within the porosity of the zeolite domains and the alumina rods are not covered with Pt. Such results confirm that our strategy successfully yield nanocomposites with metallic sites deposited selectively in the zeolite porosity (corresponding to very short distance between metallic and acidic sites) or in the close vicinity of the zeolite corresponding to a distance of about 10 nm between the two catalytic sites.

III.4. n-heptane hydrocracking

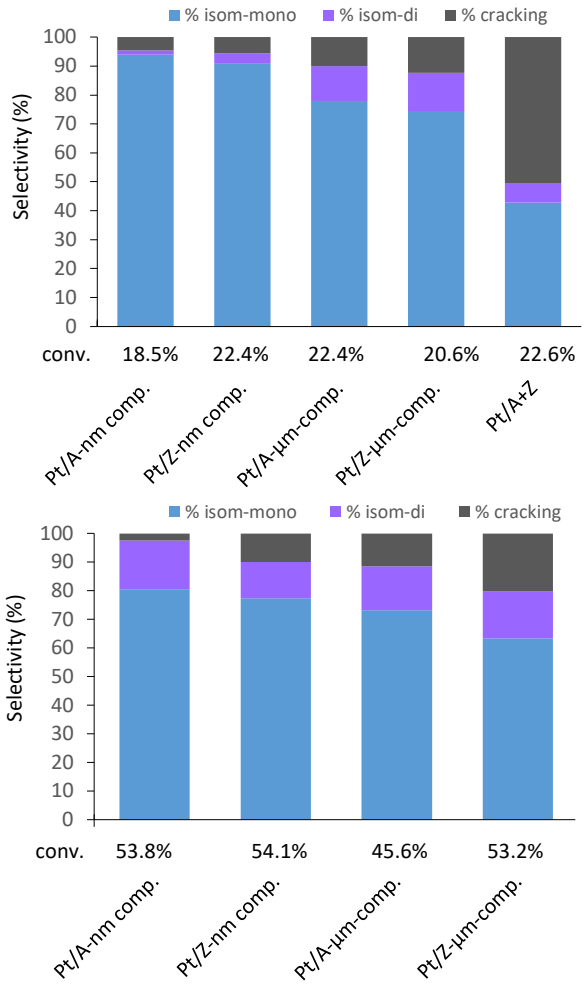

Figure 4: n-heptane hydrocracking selectivity at iso-conversion: top: 20.5±2 % conversion; bottom: 50±4 % conversion.

For the four bifunctional catalysts, the C_{Pt}/C_{H+} (ratio of metallic sites to Brønsted acid sites) is in the range 0.2-0.5 (see Tables 1&2). Hence, it largely exceeds the value of 0.03, that is usually considered as the limit value above which the activity is solely controlled by the density of acid sites (isomerization on acid site is the limiting step) and also the value of 0.1-0.15, above which the catalyst is expected to behave like an ideal bifunctional catalyst with no deactivation and high selectivity toward isomerization products [14-15]. To facilitate the comparison of the catalysts, conversions have hence been calculated for a constant amount of Brønsted acid sites of 10 µmol. Conversion *vs.* contact time curves are reported in Figure S9.

Beside the four catalysts described above, a fifth one (Pt/A + Z) was prepared by dry mechanical mixing of the 0.75 wt%Pt/Al_2O_3 sample (providing metallic sites, see Table 2) with the commercial zeolite sample (providing acid sites) in a ratio (wt. % / wt. %) 70/30. This catalyst is also expected to behave like an ideal bifunctional catalyst based on its C_{Pt}/C_{H+} ratio (0.14). However, due to its preparation protocol, the distance between metallic and acid sites in this catalyst is very high (likely tens of micrometers). For all contact times, the conversion of this catalyst is significantly lower than that of the other four catalysts. Under similar conditions (about the same amount of metallic sites), the conversion of n-heptane on the Pt/Al_2O_3 sample is negligible (below 0.5 % for all contact times) ~~as could be expected in absence of strong Brønsted acid sites for this catalyst~~. This result indicates that, although the alumina support could undergo a slight chlorination during the preparation of the catalyst (use of a chlorinated Pt precursor), it does not contribute to the acidic steps of the reaction. Hence, one can also exclude that the conversion of n-heptane observed for Pt/A+Z sample is due solely to the Pt/Al_2O_3 component. Both components (Pt/Al_2O_3 and zeolite) play a role and the lower conversion for this catalyst ~~is consistent with previous reports [14] and~~ can be assigned, in agreement with previous reports[14], to a too low intimacy of the metallic and acidic sites (under these conditions, due to the long distance that separate acid sites and metallic sites, diffusion of alkenes between acid and metallic site is the rate limiting step).

The four catalysts prepared using a zeolite-alumina composite (either µm-scale or nm-scale) as support have similar conversion (for 10 µmol of acid sites) at same contact time. More precisely, neither the size of the zeolite domains (µm-scale vs nm-scale composite) nor the location of the Pt° NPs (in the zeolite or on the alumina), significantly modify the conversion. The absence of effect of the size of the zeolite domains can be explained by the small size of the reactant molecule. Indeed, a relatively small reactant such as n-heptane, will not undergo the diffusion limitations that have be observed for larger reactants such a hexadecane in large zeolite crystals [16]. Hence, for the two sizes of zeolite domains, all acid sites are accessible to n-heptane molecules (and participate equally to its isomerization). The fact that the location of the platinum on the alumina domain (i.e., either at a few tens of nm or at a few hundreds of nm from the acid sites) rather than in the zeolite domains (i.e. at a few nms from the acid sites) has no influence on the conversion indicates that, already for these intermediate intimacies scales, the proximity between metallic and acid sites is sufficient for a fast diffusion of the alkene intermediates between metallic and acid sites. Hence, the reaction is not limited by the diffusion of the intermediate, but by the isomerization step on the acid sites, as it is expected in ideal bifunctional catalysts.

Figure 4 shows the selectivities toward monobranched isomers of n-C_7 (products obtained after one isomerisation reaction), toward di-branched isomers of n-C_7 (products obtained through two isomerisation reactions) and toward cracking products. Differences in selectivities between catalysts can be observed. In particular, the catalyst prepared by dry mechanical mixing has a very different selectivity compared to the four others (see Figure 4-top): it has a high proportion of cracking products, whereas, for the four others, the proportions of cracking products is very low and the mono-branched isomers of n-C7 dominate. Still, a

closer comparison of the selectivities, at the two conversions (ca. 20 and ca. 50%), for the four catalysts prepared using the composites as supports evidences some differences between them, with a selectivity toward one-isomerisation products that decreases in the order Pt/A-nm composite > Pt/Z-nm-composite > Pt/A-µm composite > Pt/Z-µm composite.

This comparison indicates that the type of composite (nm *vs.* µm composite) and the location of the platinum (Pt° NPs located on the alumina or on the zeolite domains) both influence the selectivity. A bifunctional acid-metal hydrocracking catalyst is regarded as ideal if the desorption of the isomerised alkylcarbenium is fast and if the resulting olefinic intermediate directly diffuses toward a metallic site to form the monobranched isomers of the starting alkane. Therefore, in an ideal hydrocracking catalyst, cracking products (and di-branched isomerisation products) are secondary reaction product s (i.e., they are formed, at high conversion, by the conversion of the primary reaction products, the mono-branched isomers) [1]. Based on this definition of an ideal bifunctional catalyst, and as emphasised by Guisnet [15], ideality in terms of selectivity is not only governed by C_{Pt}/C_{H+} but also by the number of acid sites between two metallic sites. Ideality can only be reached if the number of acid sites between two metallic sites is low enough to limit the chances of a readsorption of the isomerised alkene on an acid sites and its further isomerization.

The four catalysts prepared using the composites all have a very low selectivity toward cracking product indicating a relatively high level of ideality, whereas on the fifth one, prepared by dry mechanical mixing, crakcing products account for more than the half of the product at moderate conversion. This last catalyst has therefore a low level of ideality. This can be explained by the fact that, for this catalyst, the high distance between the zones of the catalyst where the acid sites and the metallic sites are located results in long diffusion time for the olefin intermediate in acid-sites-rich zones and hence favours their secondary and tertiary reaction with acid sites. Interestingly, this deviation to ideality is not observed for the two catalysts for which the platinum nanoparticles are located on the alumina domains of the composites, (Pt/A catalysts, for both nm-scale and µm-scale composites). On the contrary, they have a slightly higher selectivity toward mono-isomerisation products than the corresponding catalysts with a location of the platinum particles in the zeolite (Pt/Z catalysts). This result indicates that a high intimacy between the acid and the metallic sites is not required to reach the selectivity of an ideal bifunctional catalyst and that a distance between acid and metallic sites of several tens or even several hundreds of nm is still acceptable. The ideality is lost only for a very high distance between the two types of sites (as in the catalyst prepared by dry mechanical mixing). For (Pt/A-nm comp. and Pt/A-µm comp., the distance between domains bearing the metallic and the acid sites is still low enough to ensure that the probability for an alkene intermediate to be hydrogenated on metallic sites is higher than its probability to be converted to more branched isomers on acid sites. Nevertheless, this explanation does not clarify why the selectivity to isomerisation products is higher when the platinum NPs are located on the alumina phase than on the zeolite phase. Zecevic et al. recently compared the selectivities of catalysts prepared by forming Pt NPs selectively either in the Y zeolite or on the alumina binder of Y zeolite/Alumina extrudates. [4] They observed a higher selectivity toward isomerization when the Pt NPs were located on the alumina binder. They propose that a location of the Pt NPs inside the zeolite porosity increases the probability for secondary reactions because the alkenes are formed at the heart of the zeolite, where they remain trapped. Conversely, when Pt NPs are located on the alumina binder, the alkene intermediates that are formed outside the zeolite porosity mainly reacts exclusively with the acid sites located in the outer layers of the zeolite particle, and rapidly diffuses back to the metallic sides on the alumina binder. This explanation does however not fully apply to the Pt/A-(nm or µm) comp, for which all acid sites (bulk and surface acid sites) appear to be active in the isomerisation step, based on the close values of n-heptane conversions for these four catalysts (see Figure S9). Therefore, we alternatively, propose that the difference of selectivity may be due to the fact that, once the isomerised alkene diffuses outside the porosity of the zeolite, toward a metallic site (on the alumina domains) where it gets hydrogenated, the probability of these bulkier species to reenter the micropores of the zeolite is drastically reduced compared to that of the linear ones.

The degree of intimacy between the two supports also has an effect on the selectivity: the two catalysts prepared using the nanometric composite as support (Pt/A-nm comp. and Pt/Z-nm comp.) show better selectivities toward isomerisation than those prepared with the micrometric one. The origin of this difference in selectivity could be similar to that given above: the nanometric size of the zeolite particles could favour a rapid diffusion of the isomerised products outside the zeolite micropores and, their bulkiness would limit their re-entry inside the zeolite micropores.

Although the effects on the selectivity of the localisation of the Pt NPs (in the zeolite or on the alumina) and of the degree of intimacy between the zeolite and the alumina are modest, the combination of both (comparison of Pt/A-nm comp. and Pt/Z-µm comp.) leads to a very significant modification in the selectivity of the reaction.

IV. CONCLUSION

Nanometer scale zeolite-alumina composites with well-defined core-shell structure were prepared by heterocoagulation of beta zeolite and boehmite nanoparticles followed by calcination. Another composite with a micrometer scale intimacy was prepared by wet mechanical mixing of zeolite and boehmite particles.

These composites were successfully used as support for the selective deposition of the platinum precursor, either on their alumina or in their zeolite domains. This location of the platinum was preserved after calcination and reduction, thanks to optimised calcination and reduction conditions. A modification in the selectivity of n-heptane hydrocracking reaction was observed depending on the location of the Pt° NPs and on the intimacy of the zeolite and alumina phases. These modifications were assigned to a reduced probability of re-entry in the zeolite micropores for bulkier isomerised products. These results show that the selectivity of a bifunctional catalyst can be tuned by controlling its nanoscale structure.

AUTHORS INFORMATION

Corresponding Authors

juliette.blanchard@sorbonne-universite.fr, +33 144274914
olivier.durupthy@sorbonne-universite.fr, +33 144276306

Author Contributions

The manuscript was written through contributions of O.D. and J.B. authors. Others authors participated to the experimental part and the analysis of the data. All authors have given approval to the final version of the manuscript.

ASSOCIATED CONTENT

Supporting Information. Complementary (HR)TEM, STEM, XRD and N2 sorption data. This material is available free of charge via the Internet at http://pubs.acs.org.

ACKNOWLEDGMENT

This work was supported by French state funds managed by the ANR within the "Investissements d'Avenir" program (reference ANR-11-IDEX-0004-02) and more specifically within the frame-work of the Cluster of Excellence MATISSE. Authors are thankful to the French national project METSA for providing them with access to the microscope platform of IPCMS in Strasbourg.

ABBREVIATIONS

NPs: nanoparticles, DLS: Dynamic light scattering.

REFERENCES

(1) Weitkamp, J., Catalytic Hydrocracking—Mechanisms and Versatility of the Process. *ChemCatChem* **2012,** *4*, 292-306.

(2) Li, K.; Valla, J.; Garcia-Martinez, J., Realizing the Commercial Potential of Hierarchical Zeolites: New Opportunities in Catalytic Cracking. *ChemCatChem* **2014,** *6*, 46-66.

(3) Astafan, A.; Pouilloux, Y.; Patarin, J.; Bats, N.; Bouchy, C.; Jean Daou, T.; Pinard, L., Impact of Extreme Downsizing of *Bea-Type Zeolite Crystals on N-Hexadecane Hydroisomerization. *New Journal of Chemistry* **2016,** *40*, 4335-4343.

(4) Zecevic, J.; Vanbutsele, G.; de Jong, K. P.; Martens, J. A., Nanoscale Intimacy in Bifunctional Catalysts for Selective Conversion of Hydrocarbons. *Nature* **2015,** *528*, 245-248.

(5) Fang, S.-Y.; Chiang, A. S. T.; Kao, H.-M., Increasing the Productivity of Colloidal Zeolite Beta by Posthydrolysis Evaporation. *Industrial & Engineering Chemistry Research* **2010,** *49*, 12191-12196.

(6) Wu, J.-S.; Chiang, A. S. T.; Tsai, T.-C., Some Observations on the Synthesis of Colloidal Beta Zeolite from a Clear Precursor Sol. *Science of Advanced Materials* **2011,** *3*, 1011-1018.

(7) de Graaf, J.; van Dillen, A. J.; de Jong, K. P.; Koningsberger, D. C., Preparation of Highly Dispersed Pt Particles in Zeolite Y with a Narrow Particle Size Distribution: Characterization by Hydrogen Chemisorption, Tem, Exafs Spectroscopy, and Particle Modeling. *Journal of Catalysis* **2001,** *203*, 307-321.

(8) Guisnet, M.; Ayrault, P.; Datka, J., Acid Properties of Dealuminated Mordenites Studied by Ir Spectroscopy. 2. Concentration, Acid Strength and Heterogeneity of Oh Groups. *Polish journal of chemistry* **1997,** *71*, 1455-1461.

(9) Mintova, S.; Valtchev, V.; Onfroy, T.; Marichal, C.; Knözinger, H.; Bein, T., Variation of the Si/Al Ratio in Nanosized Zeolite Beta Crystals. *Microporous and Mesoporous Materials* **2006,** *90*, 237-245.

(10) Camblor, M. A.; Corma, A.; Valencia, S., Characterization of Nanocrystalline Zeolite Beta. *Microporous and Mesoporous Materials* **1998,** *25*, 59-74.

(11) Chiche, D.; Chizallet, C.; Durupthy, O.; Chaneac, C.; Revel, R.; Raybaud, P.; Jolivet, J.-P., Growth of Boehmite Particles in the Presence of Xylitol: Morphology Oriented by the Nest Effect of Hydrogen Bonding. *Physical Chemistry Chemical Physics* **2009,** *11*, 11310-11323.

(12) Samad, J. E.; Blanchard, J.; Sayag, C.; Louis, C.; Regalbuto, J. R., The Controlled Synthesis of Metal-Acid Bifunctional Catalysts: Selective Pt Deposition and Nanoparticle Synthesis on Amorphous Aluminosilicates. *Journal of Catalysis* **2016,** *342*, 213-225.

(13) Regalbuto, J. R., Strong Electrostatic Adsorption of Metals onto Catalyst Supports. In *Catalyst Preparation*, 1st ed.; CRC Press: Boca Raton, 2006; pp 297-318.

(14) Batalha, N.; Pinard, L.; Pouilloux, Y.; Guisnet, M., Bifunctional Hydrogenating/Acid Catalysis: Quantification of the Intimacy Criterion. *Catalysis Letters* **2013,** *143*, 587-591.

(15) Guisnet, M., "Ideal" Bifunctional Catalysis over Pt-Acid Zeolites. *Catalysis Today* **2013,** *218–219*, 123-134.

(16) Batalha, N.; Pinard, L.; Bouchy, C.; Guillon, E.; Guisnet, M., N-Hexadecane Hydroisomerization over Pt-Hbea Catalysts. Quantification and Effect of the Intimacy between Metal and Protonic Sites. *Journal of Catalysis* **2013,** *307*, 122-131.

SYNOPSIS TOC (Word Style "SN_Synopsis_TOC"). If you are submitting your paper to a journal that requires a synopsis graphic and/or synopsis paragraph, see the Instructions for Authors on the journal's homepage for a description of what needs to be provided and for the size requirements of the artwork.

Authors are required to submit a graphic entry for the Table of Contents (TOC) that, in conjunction with the manuscript title, should give the reader a representative idea of one of the following: A key structure, reaction, equation, concept, or theorem, etc., that is discussed in the manuscript. Consult the journal's Instructions for Authors for TOC graphic specifications.

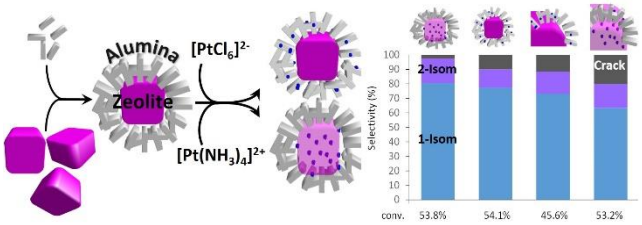

Insert Table of Contents artwork here
